Photocatalytic and photoelectrocatalytic degradation of perfluorooctanoic acid by immobilised ZnO nanoparticles using electrophoretic deposition

Amir H. Navidpour[1], Javad Safaei[2], Guojin Zhang[1], Amin Mojiri[3], Bing-Jie Ni[1], Zhenguo Huang[1], John L. Zhou[1,*]

[1]Centre for Green Technology, School of Civil and Environmental Engineering, University of Technology Sydney, 15 Broadway, Ultimo, NSW 2007, Australia

[2]Centre for Clean Energy Technology, School of Mathematical and Physical Sciences, University of Technology Sydney, 15 Broadway, Ultimo, NSW 2007, Australia

[3]Department of Civil and Environmental Engineering, Graduate School of Advanced Science and Engineering, Hiroshima University, 1-4-1 Kagamiyama, Higashihiroshima, 739-8527, Hiroshima, Japan

Corresponding author:

Prof John Zhou, junliang.zhou@uts.edu.au

Abstract

This research represented the first study of perfluorooctanoic acid (PFOA) decomposition using immobilized ZnO nanoparticles by electrophoretic deposition in photocatalysis and photoelectrocatalysis. Overall, considering process performance, application under visible light exposure, and cost-effectiveness, ZnO nanoparticles are highly promising for PFOA degradation. The effect of the probable production of sulfate radicals on PFOA photocatalytic decomposition over ZnO films was investigated by the addition of different concentrations of peroxymonosulfate (PMS). Notably, ~42% of PFOA was decomposed within 2 hours (rate constant = 0.287 h^{-1}) under UV irradiation in the presence of 0.27 g L^{-1} PMS. Importantly, the same amount of PMS initiated PFOA degradation under visible light exposure with the rate constant of 0.125 h^{-1}. In photoelectrocatalysis, the optimal ZnO film demonstrated an excellent degradation performance of ~49% within 2 hours at V = 0 (under UV irradiation). Overall, ZnO was highly promising in both photoelectrocatalysis and PMS-assisted photocatalysis, although PMS could enhance ZnO corrosion. In addition to the sulfate radicals, the photogenerated holes and superoxide radicals were among the main active species responsible for PFOA decomposition.

Keywords: Electrophoretic deposition; Perfluorooctanoic acid; Peroxymonosulfate; Photocatalysis; Photoelectrocatalysis

1. Introduction

With wide applications and environmental persistence, per- and polyfluorinated alkyl substances (PFAS) have attracted extensive attention recently.[1, 2] Perfluorooctane sulfonic acid (PFOS) and perfluorooctanoic acid (PFOA) are considered the most typical PFAS.[3] PFAS concentration has been reported in the range of pg L^{-1} to µg L^{-1} in marine, ground, surface, and drinking water[4], while significantly higher concentration up to ~1650 mg L^{-1} has been detected in some wastewater.[5] Notably, PFAS at concentrations of a few µg L^{-1} or less accumulate in organisms, and are harmful to insects, aquatic fauna, and amphibians.[6] Photocatalysis is considered an efficient method widely used for the decomposition of various pollutnsts.[7] TiO_2 is the most frequently used photocatalyst, but it has shown insignificant activity for PFOA degradation, whereas In_2O_3 and Ga_2O_3 have yielded higher efficiencies.[8-10] ZnO with its lower refractive index than TiO_2, minimizing its light scattering and providing excellent light absorption,[11] could be a potential alternative to TiO_2 for photocatalytic application. In addition to its sufficient electron mobility, abundance and chemical inertness, ZnO absorbs a larger fraction of sunlight than TiO_2.[12] Considering cost-effectiveness and efficiency, the application of ZnO as one of the most economical semiconductors in PFOA degradation should be explored.

It has been suggested that $SO_4^{\bullet-}$ radicals, which take advantages of their high durability and redox potential, could be generated through the activation of persulfate (PS) or peroxymonosulfate (PMS) by several strategies such as UV irradiation, metal ions, heat, and ultrasonication.[13, 14] Interestingly, PMS could be activated by heterogeneous catalysis as well, where it has been effectively used to improve PFOA degradation over TiO_2[15] and Ga_2O_3,[16] recently.

Photoelectrocatalysis is another prominent strategy to improve the degradation efficiency of organic pollutants by accelerating the transfer of electrons from the anode to the cathode, increasing the separation efficiency of electron/hole (e^-/h^+) pairs.[17] In addition, the degradation

capacity of pollutants could be promoted by using the bias potential in photoelectrocatalysis.[18] The application of photoelectrocatalysis necessitates immobilization of photocatalytic materials to fabricate electrodes (photoanodes). Notably, environmental photocatalysis is often criticized for the inability to recover photocatalysts (in the conventional suspended form). Therefore, the immobilization of photocatalysts has been a long-term challenge. There are several surface engineering methods to immobilize photocatalysts, but only some of them are industrial and capable of depositing solid ceramic particles. Thermal spraying and electrophoretic deposition (EPD) processes are among major methods which have been widely used for the deposition of different types of semiconductors. Specifically, conventional thermal spraying processes including plasma, flame, and high velocity oxy-fuel (HVOF) spraying have been used to immobilize ZnO,[12] TiO_2,[19] SnO_2,[20] Fe_2O_3,[21] $ZnFe_2O_4$,[22] and Zn_2SnO_4[23] for photocatalytic applications. Despite of their advantages, conventional thermal spraying processes could result in phase transformation of the feedstock material, due to the high heat input during spraying, as observed in several cases.[19, 21, 22] Furthermore, the feedstock material should be suitable for the specific thermal spray method. It has been suggested that the feedstock materials used in all thermal spray technologies should be spherical and chemically homogeneous, with a narrow particle size distribution.[24] The size of feedstock powders used in conventional thermal spraying processes (like HVOF and plasma spray) is usually restricted in the range of 10-100 μm.[25] The smallest size of the feedstock powder for all spray methods is around 10 to 15 μm.[24] Hence, Bozorgtabar et al. used agglomerated and granulated TiO_2 nanopowders as the feedstock material in HVOF[19] and air plasma spray[26] processes. EPD is considered another industrial method of surface engineering. Based on the transfer of charged solid particles to a conductive substrate under an electric field, EPD could be used for the fabrication of thick or thin coatings.[27] EPD offers exceptional benefits including short time, simplicity, homogenous films, low cost, and binder-free deposits.[28] Importantly, it is considered a non-line-of-sight process and provides the possibility to coat complex shapes.[29] Meanwhile, simple adjustment of applied

potential and deposition time could easily control morphology and thickness of the coatings fabricated by EDP.[27] Overall, EPD could be used for deposition of various types of materials including metals, ceramics, polymers, and composties.[30] Unlike conventional thermal spraying techniques, EPD process could take advantage of depositing nanoparticles without the need for their agglomeration. For instance, ZnO nanoparticles with different morphologies (i.e. nanorods and nanosheets) have been deposited on steel sheets using EPD by Mohammadi et al.[31]

Major progress has been made in the photocatalysis of PFOA in water systems, especially in using TiO_2, In_2O_3, and Ga_2O_3. Importantly, ZnO is much cheaper than In_2O_3 and Ga_2O_3. Besides, it is considered an alternative to TiO_2 in photocatalysis, while TiO_2 showed inferior performance than In_2O_3 and Ga_2O_3 for PFOA degradation.[8-10] Hence, this research aimed to investigate the photocatalytic and photoelectrocatalytic degradation of PFOA over electrophoretically deposited ZnO films (fabricated by the EPD process on fluorine doped tin oxide (FTO) coated glass) to bridge the knowledge gaps in this field of research. The research findings should help to develop ZnO-based treatment process for the continuous removal of PFOA and similar recalcitrant organic pollutants in water and wastewater.

2. Materials and methods

2.1. Materials

PFOA (95%), potassium peroxymonosulfate (Oxone), magnesium nitrate hexahydrate (99%), FTO glass (2.2 mm thickness, 7 Ω/sq surface resistivity), sodium chloride (NaCl, ≥99%), sodium sulfate (Na_2SO_4, ≥99%), benzoquinone (BQ, ≥98%), *tert*-butanol (*t*-BuOH, ≥99.7%), disodium ethylenediaminetetraacetate (EDTA-Na_2), and indium (III) oxide nano powder (In_2O_3, 99.998%) were purchased from Sigma-Aldrich, Australia. Zinc oxide nano powder (ZnO, 99.5%) was supplied from American Elements, USA. Ethanol was obtained from ChemSupply Australia Pty Ltd. PFOA solutions were prepared by dissolving the desired amount in Milli-Q water.

2.2. Photoelectrochemical measurements

A 300-W Xenon lamp (HSX-F300, Beijing NBeT Technology Co., Ltd) equipped with a cut-off filter was used to generate visible light (~400-800 nm). Four UV lamps with the wavelength of 254 nm were employed to generate UV light. Photoelectrochemical measurements were performed using a three-electrode system (CHI-760E electrochemical workstation, CH Instrument Co., China), where ZnO electrode, Pt wire, and Ag/AgCl electrode (in saturated KCl solution) were employed as the photoanode, counter electrode, and reference electrode, respectively. Photoelectrochemical measurements included linear sweep voltammetry (LSV) and transient photocurrent (I-t curves and stability).

2.3. Deposition of ZnO nanoparticles by EPD

Commercial ZnO nanoparticles were immobilised using EPD at different deposition times (1, 2, 5, 10, and 20 min), while the voltage applied was ~30 V. It has been shown that using a two-step process could reduce the size and number of cracks in EPD process.[32] Hence, the deposition process stopped after each minute and the cathode was withdrawn from the suspension and dried in air for a couple of minutes. Before immobilization, ZnO nanoparticles (~1 g) were added to ethanol (~100 mL), to which magnesium nitrate hexahydrate (~13 mg) was added as the surfactant. To provide a semi-stable colloidal solution, the mixture was sonicated for 2 h. In order to immobilise ZnO nanoparticles, FTO plates (4 cm × 6 cm) were immersed into the colloidal solution where the distance between the cathode and anode (i.e. FTO plates) was ~1.5 cm. A TTi EX354RD dual power supply was used to provide direct current (DC). To prevent sedimentation of ZnO nanoparticles, the colloidal mixture was gently stirred using small magnetic bars during the EPD process. Finally, the fabricated ZnO films were dried in air followed by the annealing treatment at 400 ˚C for 2 h. Notably, to study the surface topography

and morphology, ZnO nanoparticles were immobilized on FTO plates with the size of 1.5 cm × 1.5 cm.

2.4. Photocatalytic and photoelectrocatalytic degradation of PFOA over ZnO films

Photocatalytic and photoelectrocatalytic experiments were conducted in 100 mL of PFOA solution (~53 mg L^{-1}). Prior to light irradiation, ZnO electrodes were immersed in the initial PFOA solution for at least 0.5 h to achieve the adsorption-desorption equilibrium. A syringe was used to withdraw solution at regular time intervals; a Chromafil syringe filter (0.22 µm) was used to filter the solution before analysis. A liquid chromatograph-mass spectrometer (LC-MS 8060, Shimadzu) was used to analyse the concentration of PFOA and its degradation products. A LC column from Phenomenex (2.1 mm i.d. × 100 mm, particle size 5 µm) was used for the separation of PFOA, using Milli-Q water and methanol as mobile phases. The injection volume and flow rate were 1 µL and 0.40 mL min^{-1}, respectively. The mass to charge (*m/z*) ratio of 369.0 was used as the quantitation ion for PFOA, while the *m/z* ratios of 169.1 and 219.0 were used as the confirmation ions.

2.5. Characterization methods

Zeiss Supra 55VP scanning electron microscope (SEM) with an operating voltage of 5 kV was used to examine the surface morphology and topography of ZnO coatings. The X-ray diffraction (XRD) patterns were examined by using a Bruker D8 Discover XRD with Cu-Kα radiation at room temperature (λ = 1.5406 ˚A, 40 kV, 40 mA). Quantachrome instrument (Autosorb iQ2) was used to measure the BET specific surface area (BET_{SSA}) of ZnO and In_2O_3 nanoparticles.

3. Results and discussion

3.1. Characterization of ZnO films

A ZnO electrode was fabricated by the EPD process and analysed by XRD to clarify the stability of ZnO after immobilization. XRD patterns of the ZnO film and initial ZnO nanoparticles are compared in Figure 1. As evident, the XRD patterns are thoroughly similar, thought with different intensities, and corresponding to wurtzite phase. The higher intensity of the pattern obtained for ZnO film could be related to the increased crystallinity of the wurtzite phase due to the post thermal annealing treatment of the deposited film (at T = 400 ˚C and t = 2 h). Notably, unlike TiO_2,[26] wurtzite ZnO could take advantage of its high thermal stability where it has been stable even after plasma spraying with its considerable high temperature.[12, 20]

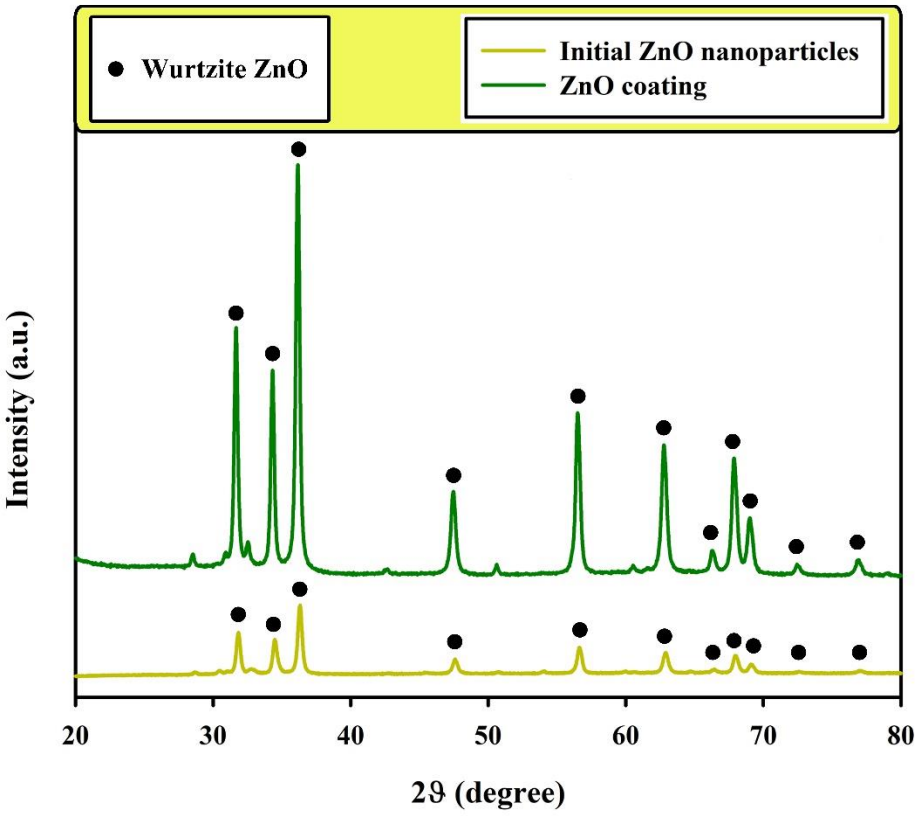

Figure 1. Comparison of the XRD patterns from ZnO film and initial ZnO nanoparticles.

Photoelectrochemical measurements were conducted for the ZnO photoanodes fabricated at different deposition times, using Na_2SO_4 (0.5 M) as the electrolyte, and the results are shown in Figure 2(a-f). The sensitivity of the electrochemical workstation was 0.001 A/V. As shown in Figure 2(a), all photoanodes were photoactivated in the range of 0-1 V (by comparing LSV

results under dark and UV irradiation). Photocurrent responses (I-t curves) of the ZnO electrodes are compared in Figure 2(b), where the photocurrent response decreased by increasing the deposition time which is related to the enhanced thickness of the photoanodes produced at longer deposition times. The photocurrent response was also measured in 45 min to evaluate the stability of the ZnO photoanodes. As shown in Figure 2(c), all photoanodes exhibited good stability, clarifying the good quality of ZnO films. As shown in Figure 2(d), similar to UV irradiation, the ZnO electrode was photoexcited in the range of 0-1 V under visible light irradiation (though marginally). The relevant I-t curves are compared in Figure 2(e), where the corresponding response under UV irradiation is considerably higher than that under visible light illumination which is related to the wide band gap energy of ZnO nanoparticles. The stability of the photocurrent responses under UV and visible light irradiation is compared in Figure 2(f), where a good stability was obtained under visible light irradiation as well. It should be noted that the irradiation intensity of UV source (32 W) was remarkably lower than that of visible light source (300 W). Overall, the photoanode fabricated at 1 min showed the highest photocurrent response and stability, it was therefore chosen to further assess the photocatalytic activity. The SEM surface morphology and topography of ZnO film fabricated at 1 min are shown in Figures 2(g) and 2(h), respectively.

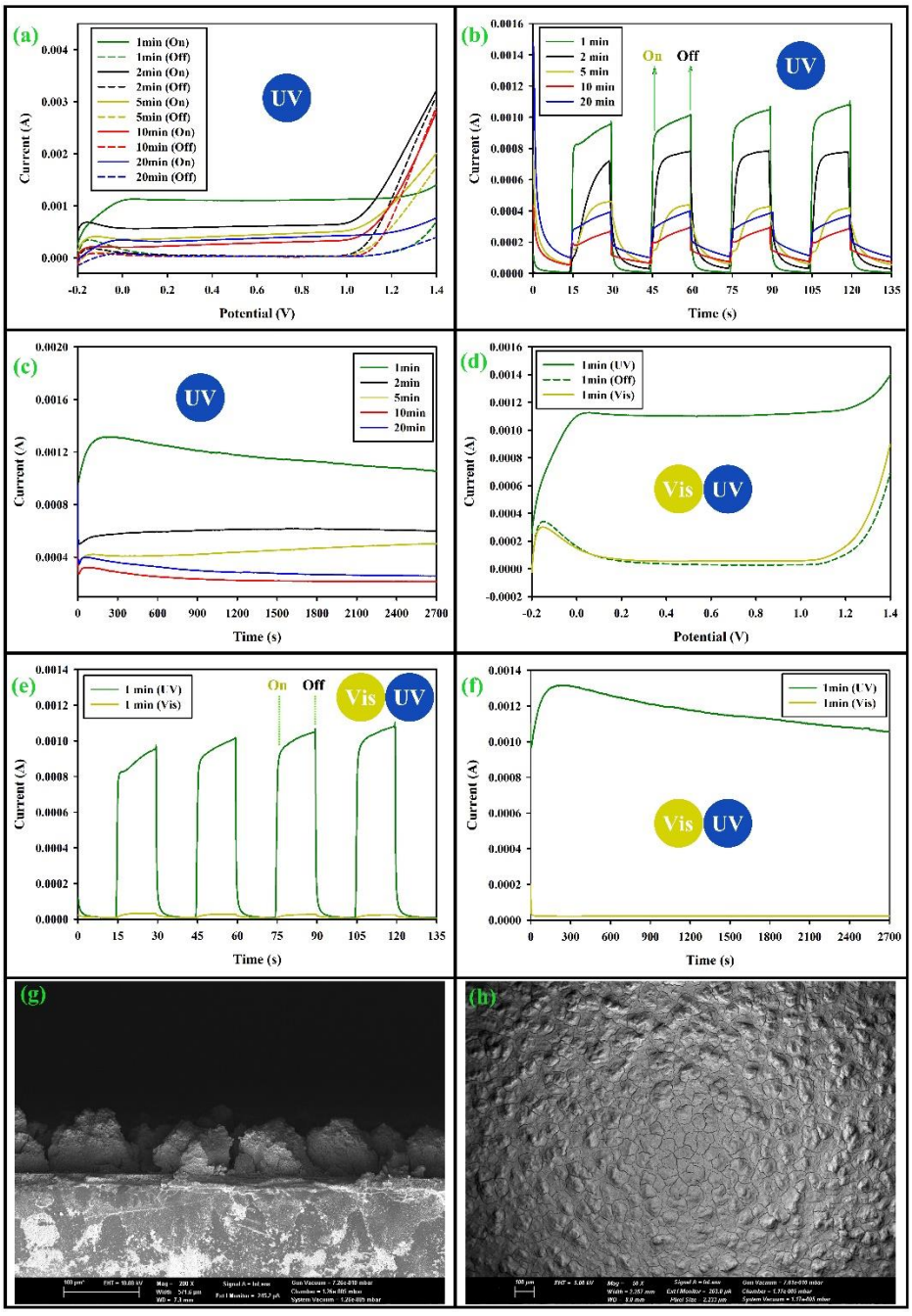

Figure 2. (a) LSV analysis under dark vs. UV irradiation (scan rate = 0.1 V s^{-1}). (b) Photocurrent response under UV irradiation (initial E = 0.6 V). (c) Stability of the ZnO photoanodes under UV irradiation (initial E = 0.6 V). (d) Comparison of the LSV results under visible and UV irradiation for the ZnO photoanode deposited in 1 min (scan rate = 0.1 V s^{-1}). (e) Comparing the photocurrent responses under visible and UV irradiation for the photoanode deposited in 1 min (initial E = 0.6 V). (f) Comparison of the stability of the ZnO photoanode deposited in 1 min under visible and UV irradiation (initial E = 0.6 V). SEM surface (g) morphology and (h) topography of the ZnO film deposited in 1 min.

209

210 **3.2. Effects of PMS and a three-electrode system on PFOA degradation**

211 Before photocatalytic experiments, to activate ZnO films to achieve high efficiency, ZnO
212 electrodes were immersed in the initial PFOA solution and irradiated by the relevant lamp (UV
213 or visible light) for at least 3 h, followed by drying in the oven. To clarify the crucial effect of
214 activation, two photocatalytic experiments were carried out using activated and non-activated
215 ZnO electrodes under similar conditions (PMS dosage = 0.27 g L^{-1}). It should be noted that the
216 activation process was carried out only with the presence of PFOA solution (without the
217 addition of PMS). Notably, a fresh PFOA solution was used to evaluate the photocatalytic
218 activity of the ZnO film after activation. As shown in Figure 3(a), non-activated ZnO film
219 showed insignificant photocatalytic activity whereas the activated film was highly efficient.
220 The photocatalytic activities of ZnO films with and without the addition of PMS under UV
221 irradiation are shown in Figures 3(b) and 3(c).

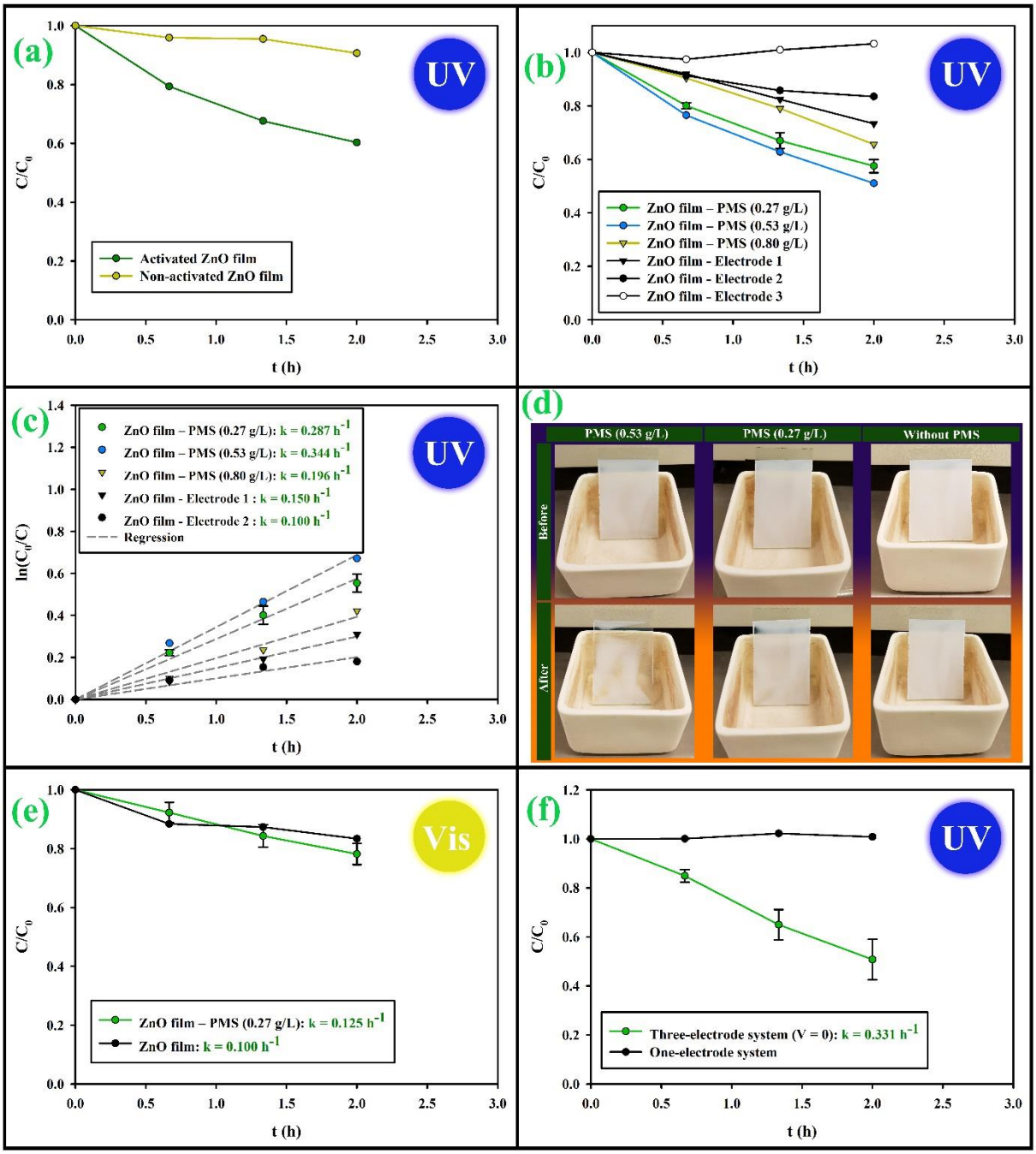

Figure 3. (a) Effect of the activation of the ZnO films on PFOA (~53 mg L^{-1}) decomposition under UV irradiation (PMS dosage: ~0.27 g L^{-1}). Plots of (b) C/C_0 and (c) apparent rate constant of PFOA degradation with and without the addition of PMS under UV irradiation. (d) The quality of ZnO coatings before and after PMS addition. (e) Plots of C/C_0 for PFOA degradation with and without the addition of PMS under visible light irradiation. (f) Photoelectrocatalytic degradation of PFOA over the ZnO film under UV illumination.

Three ZnO electrodes were used to clarify the photocatalytic activity of ZnO films without the PMS addition. Notably, they showed different performances which could be related to their different surface properties. Overall, the low efficiency of ZnO electrodes could be mainly related to the significantly reduced surface area after immobilization. For screening the optimal PMS dosage, another ZnO electrode was fabricated and used at different amounts of PMS (i.e. 0.27, 0.53, 0.80 g L^{-1}). Notably, PMS significantly improved PFOA degradation, clarifying the crucial role of $SO_4^{\bullet-}$ radicals which could be considered one of the major active species responsible for PFOA decomposition over ZnO. In addition, increasing PMS from 0.27 g L^{-1} to 0.53 g L^{-1} yielded a higher performance, but further increase of PMS to 0.80 g L^{-1} caused a reduction in PFOA degradation.

Based on the visual examination (Figure 3(d)), the quality of ZnO films showed deterioration after PMS addition, which is related to the high acidity of PMS and its concentration. Therefore, the ZnO electrodes were dried in the oven immediately after treating with PMS to maintain their quality. Notably, the pK_a of PFOA and PMS are 0.5-3.8[33] and 9.4,[34] respectively, whereas ZnO suffers from the tendency for photocorrosion especially under UV irradiation.[22] In addition to the photocorrosion, high dosages of PMS could suppress PFOA degradation due to the self-combination reaction of $SO_4^{\bullet-}$ radicals, resulting in the formation of peroxydisulfates ($S_2O_8^{2-}$) [35] which are weaker oxidants than sulfate radicals (E_0 = 2.1 and 2.6 eV, respectively).[36] Moreover, some other side reactions could lead to the consumption of oxidant species and generation of weaker oxidants.[35] As a result, further increase of PMS from 0.53 g L^{-1} to 0.80 g L^{-1} led to the significantly reduced PFOA degradation. Considering both positive and adverse effects of PMS addition, the optimal dosage of PMS was considered to be ~0.27 g L^{-1}. The corresponding apparent rate constants of PFOA decomposition were calculated and shown in Figure 3(c). It should be noted that after screening, two new electrodes were used to estimate experimental error (i.e. standard deviation) for the optimal dosage of PMS (0.27 g L^{-1}). The results of the photocatalytic decomposition of PFOA over the ZnO films under visible

light irradiation are provided in Figure 3(e). Despite of the much higher irradiation intensity of Xenon lamp than UV lamps, ZnO coating did not show significant activity under visible light, which is mainly related to the wide band gap energy of ZnO. However, the findings were still exciting from the addition of PMS (0.27 g L^{-1}), where ~22% of the initial PFOA was degraded under visible light irradiation.

The type of electrolyte and its concentration are among important factors affecting the efficiency of pollutant decomposition in photoelectrocatalysis.[37] Recently, NaCl (0.05 M) was used as the electrolyte for the photoelectrocatalytic degradation of PFOA over TiO_2 and TiO_2 modified by graphene oxide photoanodes.[38] Thus, NaCl with the same concentration was used as the electrolyte in this research. Since the photocurrent response of ZnO films did not vary significantly in the photoactivated range from 0 V to 1 V, as shown in Figures 2(a) and 2(d), the photoelectrocatalytic experiments were carried out under UV irradiation by applying the relative bias of 0 V vs. Ag/AgCl electrode. The results are shown in Figure 3(f), where using a three-electrode system considerably improved PFOA degradation. The enhanced PFOA removal using a three-electrode system could be contributed to the reduced recombination rate of charge carriers by transferring the photogenerated electrons to Pt electrode. In addition, reactive chlorine species (RCS) including $Cl^{\bullet}$ and OCl^{-}/HOCl generated in the presence of NaCl, used as an electrolyte, could also contribute in PFOA decomposition, though mainly in the final steps of PFOA degradation.[38] However, it seems that RCS did not play an important role in PFOA decomposition over the ZnO photoanode without using the three-electrode system (Figure 3(f)). The crucial effect of Pt electrode on improvement of the photocatalytic degradation of organic pollutants has also been reported by Su et al. which has been mainly attributed to the promoted dissociative adsorption of hydrogen and high electron affinity of Pt, increasing the lifetime of photogenerated chare carriers.[39] The photocurrent response of all three ZnO electrodes during the photoelectrocatalytic experiments at V = 0 (electrolyte: 0.05 M NaCl), i.e. Figure 3(f), is shown in Figure 4 to clarify the stability of ZnO photoanodes during

PFOA degradation. As evident, all electrodes showed good stability during the whole process (2 h). It is obvious that their photocurrent response decreased gradually by PFOA decomposition. It should be noted that the plunge of photocurrent at around 2400, 4800, and 7200 s is related to turning off the UV lamps at the corresponding intervals to withdraw PFOA solution for analysis by LC-MS.

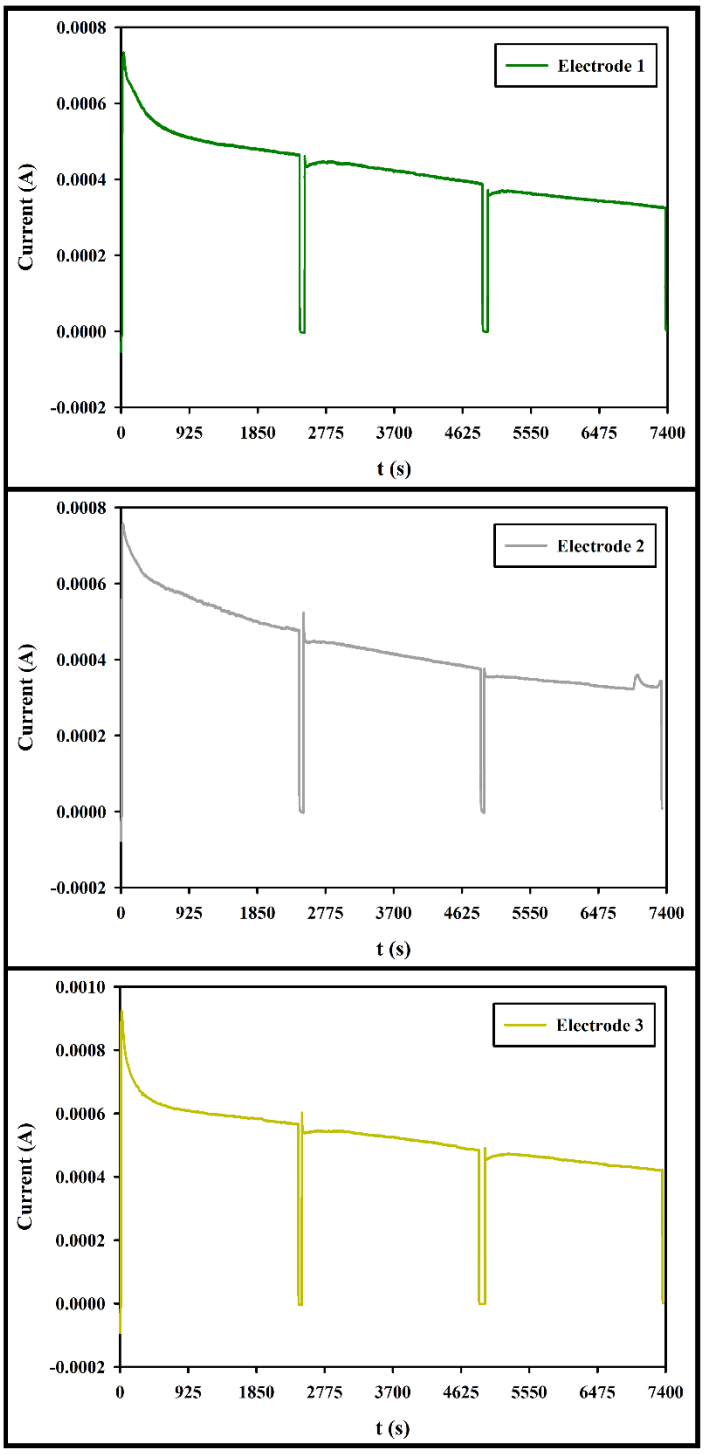

Figure 4. Stability of the ZnO electrodes during the photoelectrocatalytic experiments.

Another ZnO electrode was fabricated to evaluate its cyclic performance (three cycles) in the presence of PMS with its optimal concentration (~0.27 g L^{-1}). The visual appearance of the ZnO electrode after activation is shown in Figure 5(a). For comparison, its visual appearances after first, second, and third cycles are shown in Figures 5(b), 5(c), and 5(d), respectively. Notably, after activation of the ZnO electrode and after each cycle, the electrode was withdrawn from the solution and dried in the oven immediately. The cyclic performance of the electrode is shown in Figure 5(e). Compared with the first cycle, the activity of the electrode marginally increased in the second cycle which could be related to the adsorbed PMS on the surface of the electrode in the first cycle. However, the activity of the electrode considerably deteriorated in the third cycle which could be attributed to either the adverse effect of PMS on ZnO corrosion (as discussed previously) or the weak adhesion strength of the ZnO coatings fabricated by the EPD process. Despite of its unique features, EPD could suffer from poor coating/film adhesion.[28] Hence, although ZnO films fabricated by EPD showed very good photocatalytic and photoelectrocatalytic activities for PFOA degradation, strategies including improvement of the corrosion resistance of ZnO and application of other surface engineering methods which can deposit ZnO with high adhesion strengths (or further improvement of the adhesion strength of ZnO coatings fabricated by EPD) are still required to make the ZnO films more robust for practical applications.

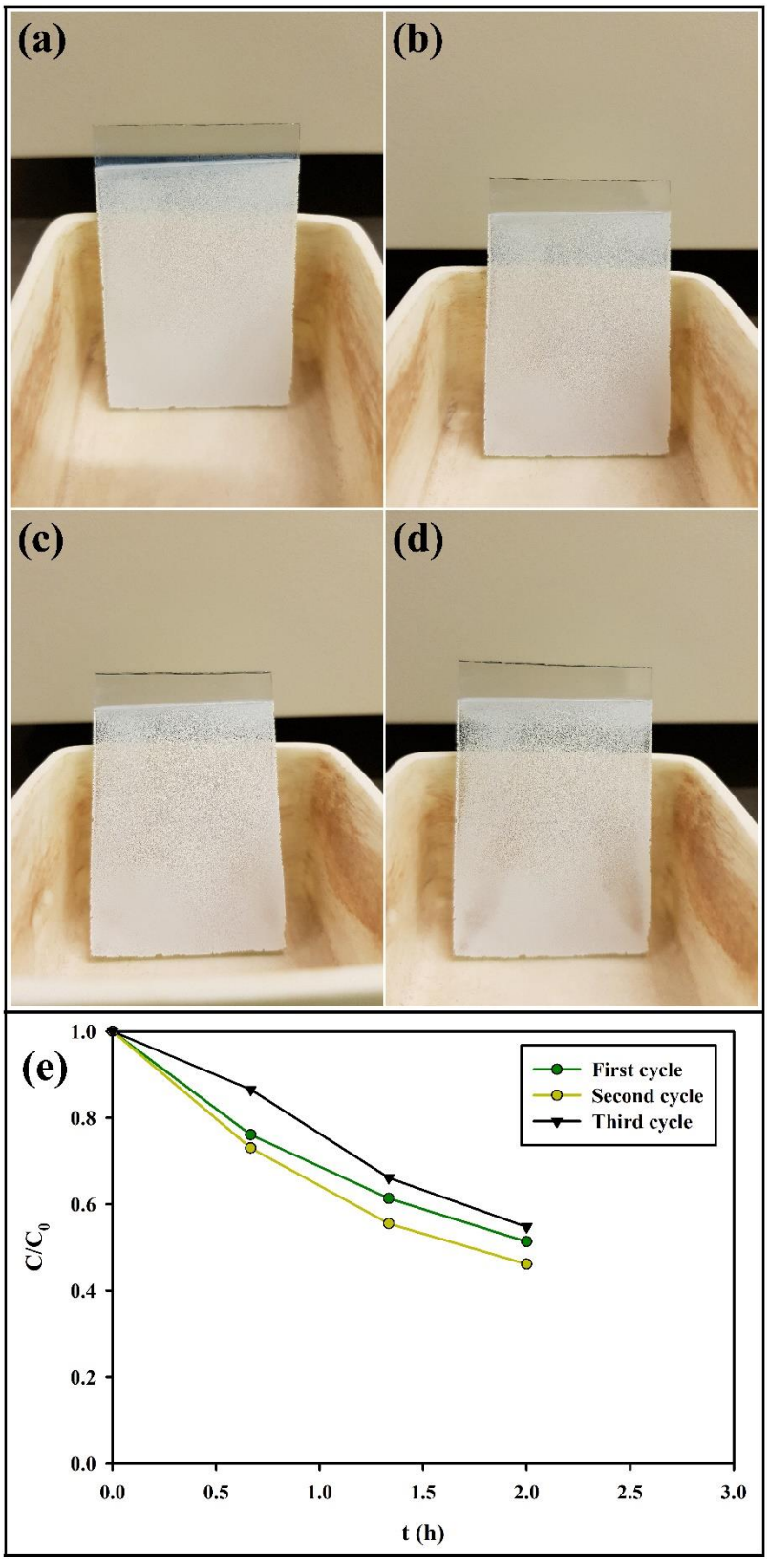

Figure 5. Visual appearance of the ZnO electrode after (a) activation, (b) first cycle, (c) second cycle, and (d) third cycle. (e) Cyclic performance of the ZnO electrode in the presence of PMS (~0.27 g L^{-1}) under UV irradiation.

The effect of PMS on PFOA degradation in the absence of ZnO was also investigated under both UV and visible light irradiation (Figure S1(a)). The vessels used for evaluation of the photocatalytic/photoelectrocatalytic decomposition of PFOA over ZnO are shown in Figure S1(b). Notably, a quartz reaction vessel with a holder was used for the ZnO electrodes, where they relied on the holder during the photocatalytic experiments; and the light source (UV or visible) was irradiated from the front side of the ZnO electrodes (Figure S1(b, i)). Since powders could become stuck in the holder, a simple vessel was used for evaluation of the photocatalytic activity of suspended ZnO nanoparticles (Figure S1(b, ii)). A wider vessel was used to evaluate the effect of PMS in the absence of ZnO (Figure S1(b, iii)). It reduces the depth of PFOA solution since the initial volume was ~100 mL in all cases. As shown in Figure S1(a), neither UV nor visible light were able to highly degrade PFOA in the absence of ZnO (even by increasing the irradiation time). Hence, PMS alone (in the absence of ZnO as photocatalyst) did not play an important role in PFOA degradation. Similarly, as reported by Xu et al., only 18% of PFOA was decomposed under UV irradiation (254 nm) within 3 h when using only PMS.[16]

Another ZnO electrode was fabricated to evaluate the effect of irradiation time on the photocatalytic decomposition of PFOA under UV irradiation with the addition of PMS (~0.27 g L^{-1}). As shown in Figure S2, the decomposition efficiency reached ~64% after 4.5 h while it was ~42% after 2 h (Figure 3(b)). It has been reported that the total degradation of PFOA could be achieved in PMS-assisted photocatalysis. For instance, PFOA was completely degraded within 2 h when using the molar ratio of 1:1 between Ga_2O_3 and PMS, while only ~58% of PFOA was degraded in 3 h by using only Ga_2O_3 powder.[16] Considering these findings, it is estimated that the total decomposition of PFOA over the ZnO film needs a prolonged time. It should be also noted that the specific surface area of the catalyst reduces after deposition on a substrate which is one of the major drawbacks of immobilization.

The photocatalytic and photoelectrocatalytic activities of several semiconductors used for PFOA decomposition are compared in Table 1, where photoelectrocatalysis is more efficient

than custom photocatalysis in all cases. Notably, PFOA concentration in the range of ~50 mg L^{-1} is usually higher than that detected in the polluted water,[15] but the initial PFOA concentration in the range of mg L^{-1} has been used by other researchers (Table 1) which could be related to the usually higher efficiency of degradation at higher initial concentrations. However, it should be noted that the effect of the initial PFOA concentration on its degradation highly depends on the type of catalyst. For instance, increasing the initial concentration from 20 mg L^{-1} to 40 mg L^{-1} and 60 mg L^{-1} improved the rate constant of PFOA decomposition using Pt-, Ag-, and Pd-modified TiO_2 whereas the same order of increase in the initial concentration showed a reduction in the degradation rate constant using pure TiO_2.[40]

348 Table 1. Comparison between photocatalytic and photoelectrocatalytic activity of PFOA degradation over different semiconductors.

Catalyst/Electrode	**Light source**	**$[PFOA]_0$ (mg L^{-1})**	**Photocatalysis**	**Photoelectrocatalysis**		**Reference**
				Efficiency	**Electrolyte**	
TiO_2 powder	Xenon lamp (300 W, 400-770 nm)	50	0.028 h^{-1} (~20% in 8 h)	-	-	[15]
TiO_2 powder	UV (254 nm)	41.4	0.045 h^{-1} (~16% in 4 h)	-	-	[8]
In_2O_3 powder	UV (254 nm)	41.4	0.378 h^{-1} (~80% in 4 h)	-	-	[8]
In_2O_3 microspheres	UV (254 nm)	30	~100% in 20 min	-	-	[41]
In_2O_3 nanoplates	UV (254 nm)	30	~100% in 40 min	-	-	[41]
In_2O_3 nanocubes	UV (254 nm)	30	~100% in 2 h	-	-	[41]
ZnO powder	UV (32 W, 254 nm)	53	0.090 h^{-1} (~19% in 2 h)	-	-	This work
TiO_2 electrode	100 mW/cm^2	9.9	0.006 h^{-1} (~2% in 2 h)	0.03 h^{-1} (~5% in 2 h)	Na_2SO_4 (0.1 M)	[42]
TiO_2 electrode	UV (16 W, 254 nm)	5	-	0.378 h^{-1} (~46% in 2 h)	NaCl (0.05 M)	[38]
TiO_2/GO electrode	UV (16 W, 254 nm)	5	0	0.372 h^{-1} (~43% in 2 h)	NaCl (0.05 M)	[38]
TiO_2 electrode	Low pressure Hg lamp (100 W)	40	~14% in 2 h	~44% in 2 h	H_2SO_4 (0.1 M)	[43]
ZnO electrode	UV (32 W, 254 nm)	53	0-27%	0.331 h^{-1} (~49% in 2 h)	NaCl (0.05 M)	This work

349 Note: GO (graphene oxide)

3.3. PFOA photodegradation mechanism

The crucial role of sulfate radicals on PFOA decomposition over ZnO films was clarified in the previous section by PMS adding. To elucidate other active species, three reagents including t-BuOH, BQ, and EDTA-Na_2 were added to the initial PFOA solution to scavenge $^{\bullet}OH$, $O_2^{\bullet-}$, and the photogenerated holes (h^+), respectively. For simplicity, suspended ZnO nanoparticles (0.53 g L^{-1}) were used for the analysis of the active species and intermediates. As shown in Figure S3(a), the photocatalytic activity of ZnO nanoparticles was quenched considerably by the addition of EDTA-Na_2 and BQ, clarifying the crucial role of h^+ and $O_2^{\bullet-}$ in PFOA decomposition, whereas the addition of t-BuOH (even at high concentrations up to 0.1 and 0.2 M) did not reduce PFOA decomposition. Notably, using high concentrations of t-BuOH could increase PFOA degradation because of its less polarity than water, leading to the higher reactivity of superoxide radicals.[44] The intermediates formed during the photocatalytic degradation of PFOA could include PFHpA, PFHxA, PFPeA, PFBA, PFPrA, and TFA (in PMS-assisted photocatalysis using ZnO), but the shorter chains of PFOA (especially the last ones including PFBA, PFPrA, and TFA) could be hardly detected (due to their low concentration) as reported by Xu et al., where TiO_2 was used as the photocatalyst.[15] The time dependence of the first three shorter chains of PFOA is shown in Figure S3(b), where PFHpA, PFHxA, and PFPeA could be respectively considered the first, second, and third generated intermediates. Overall, it is estimated that the photodecomposition of PFOA over ZnO could follow a stepwise manner from PFOA to its shorter chains including PFHpA, PFHxA, and PFPeA. The stepwise manner of PFOA degradation has been reported in several cases using various photocatalysts.[15, 16, 36]

The adsorption of the organic pollutant on the catalyst surface is of high importance in photocatalysis. Thus, the adsorption capacity of PFOA over ZnO nanoparticles was measured and compared to that of In_2O_3 nanoparticles (for control). To measure PFOA adsorption, the catalysts were stirred in PFOA solution (~53 mg L^{-1}) for 1.5 h in the dark. To clearly

discriminate the adsorption capacity of PFOA over catalysts, the catalysts dosage was considered approximately 4 times higher than that used in the photocatalytic experiments (i.e. 0.53 g L^{-1} as mentioned previously). The adsorption capacity of PFOA over In_2O_3 nanoparticles was around 1.6 times higher than that over ZnO nanoparticles (~39.6% vs. ~24.8%), whereas the BET_{SSA} of ZnO nanoparticles was around 4.3 times higher than that of In_2O_3 nanoparticles (~30 m^2 g^{-1} vs. ~7 m^2 g^{-1}). For control, the photocatalytic activity of suspended In_2O_3 nanoparticles for PFOA degradation was also investigated under UV irradiation (Figure S4). Considering Figure S3(a), it is concluded that ZnO nanoparticles were more promising (~21% degradation within 2 h) than In_2O_3 nanoparticles (~14% degradation within 4 h). Hence, it seems that the lower adsorption capacity of PFOA over ZnO nanoparticles did not play an important role in the promising performance of ZnO for PFOA degradation.

4. Conclusions

The potential degradation of PFOA (as one of the most persistent organic pollutants) has been examined using immobilized ZnO nanoparticles (as one of the most economical semiconductors) in photocatalysis and photoelectrocatalysis modes. The probable production of sulfate radicals by the addition of PMS significantly improved PFOA decomposition over ZnO films, where the high apparent rate constants of 0.287 h^{-1} and 0.125 h^{-1} were achieved by the addition of PMS (0.27 g L^{-1}) under UV and visible light irradiation, respectively. Overall, considering cost-effectiveness, degradation efficiency, and the potential of use under visible light, ZnO films are very promising as the candidate photocatalyst for PFOA decomposition. In addition to the strong effect of PMS, ZnO electrodes produced by EPD offered high efficiency using the three-electrode system (rate constant = 0.331 h^{-1}). Hence, ZnO films have demonstrated high capability for PFOA decomposition in both photocatalysis and photoelectrocatalysis under UV irradiation. Further research is required to develop more efficient visible light-activated photoanodes with improved photocorrosion resistance.

Acknowledgements

This work is supported by the University of Technology Sydney.

References

1. J. Becanova, Z. S. S. L. Saleeba, A. Stone, A. R. Robuck, R. H. Hurt and R. Lohmann, A graphene-based hydrogel monolith with tailored surface chemistry for PFAS passive sampling, *Environ. Sci. Nano*, 2021, **8**, 2894-2907.
2. X. Tan, G. Chen, D. Xing, W. Ding, H. Liu, T. Li and Y. Huang, Indium-modified Ga_2O_3 hierarchical nanosheets as efficient photocatalysts for the degradation of perfluorooctanoic acid, *Environ. Sci. Nano*, 2020, **7**, 2229-2239.
3. W. Wang, H. Shao, C. Sun, X. Jiang, S. Zhou, G. Yu and S. Deng, Preparation of magnetic covalent triazine frameworks by ball milling for efficient removal of PFOS and PFOA substitutes from water, *Environ. Sci. Nano*, 2022, **9**, 1466-1475.
4. O. C. Olatunde, A. T. Kuvarega and D. C. Onwudiwe, Photo enhanced degradation of polyfluoroalkyl and perfluoroalkyl substances, *Heliyon*, 2020, **6**, e05614.
5. C. Y. Tang, Q. S. Fu, A. P. Robertson, C. S. Criddle and J. O. Leckie, Use of reverse osmosis membranes to remove perfluorooctane sulfonate (PFOS) from semiconductor wastewater, *Environmen. Sci. Technol.*, 2006, **40**, 7343-7349.
6. H. Brunn, G. Arnold, W. Körner, G. Rippen, K. G. Steinhäuser and I. Valentin, PFAS: forever chemicals-persistent, bioaccumulative and mobile. Reviewing the status and the need for their phase out and remediation of contaminated sites, *Environ. Sci. Eur.*, 2023, **35**, 20.
7. X. Liu, B. Xu, X. Duan, Q. Hao, W. Wei, S. Wang and B.-J. Ni, Facile preparation of hydrophilic In_2O_3 nanospheres and rods with improved performances for photocatalytic degradation of PFOA, *Environ. Sci. Nano*, 2021, **8**, 1010-1018.

8. X. Li, P. Zhang, L. Jin, T. Shao, Z. Li and J. Cao, Efficient photocatalytic decomposition of perfluorooctanoic acid by indium oxide and its mechanism, *Environ. Sci. Technol.*, 2012, **46**, 5528-5534.
9. B. Xu, M. B. Ahmed, J. L. Zhou, A. Altaee, M. Wu and G. Xu, Photocatalytic removal of perfluoroalkyl substances from water and wastewater: Mechanism, kinetics and controlling factors, *Chemosphere*, 2017, **189**, 717-729.
10. Z. Li, P. Zhang, J. Li, T. Shao, J. Wang and L. Jin, Synthesis of In_2O_3 porous nanoplates for photocatalytic decomposition of perfluorooctanoic acid (PFOA), *Catal. Commun.*, 2014, **43**, 42-46.
11. S. Kumar, A. Kumar, A. Kumar and V. Krishnan, Nanoscale zinc oxide based heterojunctions as visible light active photocatalysts for hydrogen energy and environmental remediation, *Catal. Rev.*, 2020, **62**, 346-405.
12. A. H. Navidpour, Y. Kalantari, M. Salehi, H. R. Salimijazi, M. Amirnasr, M. Rismanchian and M. Azarpour Siahkali, Plasma-sprayed photocatalytic zinc oxide coatings, *J. Therm. Spray Technol.*, 2017, **26**, 717-727.
13. H. Shao, X. Zhao, Y. Wang, R. Mao, Y. Wang, M. Qiao, S. Zhao and Y. Zhu, Synergetic activation of peroxymonosulfate by Co_3O_4 modified g-C_3N_4 for enhanced degradation of diclofenac sodium under visible light irradiation, *Appl. Catal. B: Environ.*, 2017, **218**, 810-818.
14. M. Sabri, A. Habibi-Yangjeh, S. Rahim Pouran and C. Wang, Titania-activated persulfate for environmental remediation: the-state-of-the-art, *Catal. Rev.*, 2021, DOI: 10.1080/01614940.2021.1996776, 1-56.
15. B. Xu, M. B. Ahmed, J. L. Zhou and A. Altaee, Visible and UV photocatalysis of aqueous perfluorooctanoic acid by TiO_2 and peroxymonosulfate: Process kinetics and mechanistic insights, *Chemosphere*, 2020, **243**, 125366.

16. B. Xu, J. L. Zhou, A. Altaee, M. B. Ahmed, M. A. H. Johir, J. Ren and X. Li, Improved photocatalysis of perfluorooctanoic acid in water and wastewater by Ga_2O_3/UV system assisted by peroxymonosulfate, *Chemosphere*, 2020, **239**, 124722.
17. A. H. Navidpour, A. Hosseinzadeh, J. L. Zhou and Z. Huang, Progress in the application of surface engineering methods in immobilizing TiO_2 and ZnO coatings for environmental photocatalysis, *Catal. Rev.*, 2021, DOI: 10.1080/01614940.2021.1983066, 1-52.
18. H. Tang, Q. Shang, Y. Tang, X. Yi, Y. Wei, K. Yin, M. Liu and C. Liu, Static and continuous flow photoelectrocatalytic treatment of antibiotic wastewater over mesh of TiO_2 nanotubes implanted with g-C_3N_4 nanosheets, *J. Hazard. Mater.*, 2020, **384**, 121248.
19. M. Bozorgtabar, M. Rahimipour and M. Salehi, Novel photocatalytic TiO_2 coatings produced by HVOF thermal spraying process, *Mater. Lett.*, 2010, **64**, 1173-1175.
20. A. H. Navidpour, M. Fakhrzad, M. Tahari and S. Abbasi, Novel photocatalytic coatings based on tin oxide semiconductor, *Surf. Eng.*, 2019, **35**, 216-226.
21. A. H. Navidpour, M. Salehi, M. Amirnasr, H. R. Salimijazi, M. Azarpour Siahkali, Y. Kalantari and M. Mohammadnezhad, Photocatalytic iron oxide coatings produced by thermal spraying process, *J. Therm. Spray Technol.*, 2015, **24**, 1487-1497.
22. A. H. Navidpour, M. Salehi, H. R. Salimijazi, Y. Kalantari and M. Azarpour Siahkali, Photocatalytic activity of flame-sprayed coating of zinc ferrite powder, *J. Therm. Spray Technol.*, 2017, **26**, 2030-2039.
23. A. H. Navidpour and M. Fakhrzad, Photocatalytic activity of Zn_2SnO_4 coating deposited by air plasma spraying, *Appl. Surf. Sci. Adv.*, 2021, **6**, 100153.
24. L. Łatka, L. Pawłowski, M. Winnicki, P. Sokołowski, A. Małachowska and S. Kozerski, Review of functionally graded thermal sprayed coatings, *Appl. Sci.*, 2020, **10**, 5153.
25. G. Mittal and S. Paul, Suspension and solution precursor plasma and HVOF spray: A review, *J. Therm. Spray Technol.*, 2022, **31**, 1443-1475.

26. M. Bozorgtabar, M. Rahimipour, M. Salehi and M. Jafarpour, Structure and photocatalytic activity of TiO_2 coatings deposited by atmospheric plasma spraying, *Surf. Coat. Technol.*, 2011, **205**, S229-S231.
27. K. E. Fox, N. L. Tran, T. A. Nguyen, T. T. Nguyen and P. A. Tran, in *Biomaterials in Translational Medicine*, eds. L. Yang, S. B. Bhaduri and T. J. Webster, Academic Press, 2019, DOI: https://doi.org/10.1016/B978-0-12-813477-1.00008-6, pp. 163-189.
28. B. K. Chakrabarti, M. Gençten, G. Bree, A. H. Dao, D. Mandler and C. T. J. Low, Modern practices in electrophoretic deposition to manufacture energy storage electrodes, *Int. J. Energy Res.*, 2022, **46**, 13205-13250.
29. M. Roy, A. Bandyopadhyay and S. Bose, in *Materials for Bone Disorders*, eds. S. Bose and A. Bandyopadhyay, Academic Press, 2017, DOI: https://doi.org/10.1016/B978-0-12-802792-9.00006-9, pp. 265-314.
30. H. V. Ramos Avilez, D. A. Castilla Casadiego, A. L. Vega Avila, O. J. Perales Perez and J. Almodovar, in *Chitosan Based Biomaterials Volume 1*, eds. J. A. Jennings and J. D. Bumgardner, Woodhead Publishing, 2017, DOI: https://doi.org/10.1016/B978-0-08-100230-8.00011-X, pp. 255-293.
31. E. Mohammadi, M. Aliofkhazraei and A. S. Rouhaghdam, In-situ study of electrophoretic deposition of zinc oxide nanosheets and nanorods, *Ceram. Int.*, 2018, **44**, 1471-1482.
32. W.-H. Chiu, K.-M. Lee and W.-F. Hsieh, High efficiency flexible dye-sensitized solar cells by multiple electrophoretic depositions, *J. Power Sources*, 2011, **196**, 3683-3687.
33. F. A. Hussain, S. E. Janisse, M. C. Heffern, M. Kinyua and J. M. Velázquez, Adsorption of perfluorooctanoic acid from water by pH-modulated Brönsted acid and base sites in mesoporous hafnium oxide ceramics, *iScience*, 2022, **25**, 104138.
34. L. Wu, Y. Lin, Y. Zhang, P. Wang, M. Ding, M. Nie, C. Yan and S. Chen, $Ca(OH)_2$-mediated activation of peroxymonosulfate for the degradation of bisphenol S, *RSC Adv.*, 2021, **11**, 33626-33636.

35. K. Zhu, J. Wang, Y. Wang, C. Jin and A. S. Ganeshraja, Visible-light-induced photocatalysis and peroxymonosulfate activation over $ZnFe_2O_4$ fine nanoparticles for degradation of Orange II, *Catal. Sci. Technol.*, 2016, **6**, 2296-2304.
36. D. Wu, X. Li, J. Zhang, W. Chen, P. Lu, Y. Tang and L. Li, Efficient PFOA degradation by persulfate-assisted photocatalytic ozonation, *Sep. Purif. Technol.*, 2018, **207**, 255-261.
37. Y. Lee and J. Khim, Effects of electrolyte concentration and anion identity on photoelectrochemical degradation of phenol: Focusing on the change at the photoanode/solution interface, *J. Environ. Chem. Eng.*, 2021, **9**, 106717.
38. J.-S. Yang, W. W.-P. Lai, S. C. Panchangam and A. Y.-C. Lin, Photoelectrochemical degradation of perfluorooctanoic acid (PFOA) with GOP25/FTO anodes: Intermediates and reaction pathways, *J. Hazard. Mater.*, 2020, **391**, 122247.
39. Y.-F. Su and T.-C. Chou, Comparison of the photocatalytic and photoelectrocatalytic decolorization of methyl orange on sputtered TiO_2 thin films, *Z. fur Naturforsch. B*, 2005, **60**, 1158-1167.
40. M. Li, Z. Yu, Q. Liu, L. Sun and W. Huang, Photocatalytic decomposition of perfluorooctanoic acid by noble metallic nanoparticles modified TiO_2, *Chem. Eng. J.*, 2016, **286**, 232-238.
41. Z. Li, P. Zhang, T. Shao, J. Wang, L. Jin and X. Li, Different nanostructured In_2O_3 for photocatalytic decomposition of perfluorooctanoic acid (PFOA), *J. Hazard. Mater.*, 2013, **260**, 40-46.
42. Y. Zhou, Y. Lee, Y. Ren, M. Cui and J. Khim, Quantification of perfluorooctanoic acid decomposition mechanism applying negative voltage to anode during photoelectrochemical process, *Chemosphere*, 2021, **284**, 131311.
43. Y.-P. Peng, H. Chen and C. P. Huang, The synergistic effect of photoelectrochemical (PEC) reactions exemplified by concurrent perfluorooctanoic acid (PFOA) degradation and

hydrogen generation over carbon and nitrogen codoped TiO_2 nanotube arrays (C-N-TNTAs) photoelectrode, *Appl. Catal. B: Environ.*, 2017, **209**, 437-446.

44. X. He, B. Sun, M. He, H. Chi, Z. Wang, W. Zhang and J. Ma, Highly efficient simultaneous catalytic degradation and defluorination of perfluorooctanoic acid by the H_2O_2-carbon/MnO_2 system generating O^{2-} and OH synchronously, *Appl. Catal. B: Environ.*, 2020, **277**, 119219.